Modeling Selenate Adsorption Behavior on Oxides, Clay Minerals, and Soils Using the Triple Layer Model

Sabine Goldberg

Abstract: Selenate adsorption behavior was investigated on amorphous aluminum oxide; amorphous iron oxide; clay minerals kaolinites, montmorillonites, and illite; and 18 soil samples from Hawaii and the Southwestern and Midwestern regions of the United States as a function of solution pH. Selenate adsorption decreased with increasing solution pH. The triple layer model, a chemical surface complexation model, was able to describe Se (VI) adsorption as a function of solution pH by simultaneously optimizing either two outer-sphere Se(VI) surface complexation constants or one inner-sphere and one outer-sphere Se(VI) surface complexation constant. The fit of the triple layer model to Se(VI) adsorption by oxides, clay minerals, and soils was excellent, as evidenced by very low values of the model variance goodness-of-fit criterion. The predominantly outer-sphere Se(VI) surface speciation predicted using the triple layer model was in agreement with the weak adsorption behavior previously observed for Se(VI) using electrophoretic mobility measurements and ionic strength dependence of adsorption. Direct spectroscopic investigations of Se(VI) surface configurations are needed to corroborate the species predicted by the triple layer modeling approach.

Key Words: Selenium, selenite, kaolinite, illite

(*Soil Sci* 2014;179: 568–576)

Selenium (Se) is an essential micronutrient element for animal nutrition. It has a very narrow range between deficiency and toxicity symptoms, making it a potentially toxic trace element for humans, livestock, wildlife, and aquatic species. Selenium concentrations in soils and waters can become elevated because of disposal of coal and fly ash, discharges from mining operations and petroleum refineries, mineral dissolution and oxidation, and drainage of seleniferous soils (Girling, 1984). Average soil Se concentrations range from less than 0.1 to 2 mg/kg, whereas seleniferous soils contain Se at levels ranging from 2 to 300 mg/kg (Adriano, 2001). The bioaccumulation process can produce vegetation toxic for grazing ruminant animals on seleniferous soils (Lakin, 1961) and for waterfowl in ponds receiving drainage waters high in Se (Ohlendorf et al., 1986).

The major inorganic Se species found in groundwaters, irrigation waters, and soil solutions are the oxidation states: selenite (Se (IV)), under reducing conditions, and selenate (Se(VI)), under oxidizing conditions (Adriano, 2001). The kinetics of Se(IV) oxidation and Se(VI) reduction are slow, so that both Se species often coexist in soil solution (Masscheleyn et al., 1990). The predominant species of Se(IV) found at environmental pH values are $HSeO_3^-$ and SeO_3^{2-} because selenious acid is a weak diprotic acid with dissociation constants: $pK_{a1} = 2.46$ and $pK_{a2} = 7.31$ at 298 K (Weast et al., 1984). The completely dissociated species SeO_4^{2-} is the only Se (VI) species present in most natural pH environments because selenic acid is a strong acid with a second dissociation constant: $pK_{a2} = 1.92$ at 298 K (Weast et al., 1984). Selenium toxicity is dependent on oxidation state, with the more reduced Se(IV) species considered to be more toxic (Fernandez et al., 1993).

Adsorption reactions on surfaces of soil minerals can attenuate solution Se concentrations. Selenium adsorption behavior has been studied on a wide range of adsorbent surfaces including oxide minerals, clay minerals, carbonates, and whole soils. The extent of Se adsorption is a function of redox state, soil solution pH, and soil mineral type. The pH-dependent adsorption behavior is similar for both Se redox states: exhibiting a maximum at low pH and decreasing adsorption with increasing solution pH on both iron oxides (Balistrieri and Chao, 1987; Duc et al., 2003) and aluminum oxide (Goldberg, 2014). However, the amount of Se(VI) adsorption was observed to be much less than that of Se(IV) adsorption (Balistrieri and Chao, 1987; Duc et al., 2003). Selenate adsorption also decreased much more rapidly with increasing solution pH than did Se(IV) adsorption (Balistrieri and Chao, 1987; Goldberg, 2014).

Similar pH-dependent adsorption behavior as on oxide minerals was also observed for Se(IV) and Se(VI) on tropical soils from Brazil (Gabos et al., 2014). Both Se(IV) and Se(VI) adsorption maxima on these tropical soils showed a highly significant statistical correlation with Al and Fe oxide contents. In contrast, calcareous arid zone soils, containing much smaller amounts of extractable oxides, adsorbed Se(IV) but virtually no Se(VI) as a function of solution pH (Neal and Sposito, 1989). Selenate adsorption was observed on some acid Finnish soils (Vuori et al., 1989, 1994) but not on others (Yläranta, 1983). Selenite adsorption on a set of Northeastern, Southeastern, and Midwestern US soils was on average three times greater than Se(VI) adsorption (Goldberg et al., 2008a).

Macroscopic evidence for inner-sphere surface complexation of Se(IV) was provided by the lack of ionic strength dependence of its adsorption behavior on amorphous Fe oxide, goethite (Su and Suarez, 2000), hematite (Duc et al., 2003), maghemite (Jordan et al., 2014), and gibbsite (Goldberg, 2014). Selenate adsorption, on the other hand, exhibited pronounced decreases in adsorption with increasing ionic strength on amorphous Fe oxide, goethite (Su and Suarez, 2000), maghemite (Jordan et al., 2013), and gibbsite (Goldberg, 2014): macroscopic evidence for outer-sphere surface complexation. Electrophoretic mobility measurements of point of zero charge (PZC) also provide macroscopic information on ion adsorption mechanisms. Shifts in PZC on adsorption of Se(IV) on goethite (Hansmann and Anderson, 1985), amorphous Fe oxide (Su and Suarez, 2000), maghemite (Jordan et al., 2014), alumina (Rajan, 1979), and gibbsite (Goldberg, 2014) provide indirect evidence for inner-sphere surface complex formation. Selenate adsorption on goethite, amorphous Fe oxide (Su and Suarez, 2000), and gibbsite (Goldberg, 2014) resulted in PZC shifts, whereas Se(VI) adsorption on maghemite did not (Jordan et al., 2013). Thus, the strength of Se(VI) adsorption seems to vary with oxide mineral type.

U.S. Department of Agriculture–Agricultural Research Service, U.S. Salinity Laboratory, Riverside, California, USA.
Address for correspondence: Dr. Sabine Goldberg, U.S. Department of Agriculture–Agricultural Research Service, U.S. Salinity Laboratory, 450 W. Big Springs Rd, Riverside, CA 92507, USA. E-mail: sabine.goldberg@ars.usda.gov
Financial Disclosures/Conflicts of Interest: None reported.
Received September 8, 2014.
Accepted for publication December 29, 2014.

ISSN: 0038-075X
DOI: 10.1097/SS.0000000000000097

Spectroscopic techniques provide direct microscopic evaluation of ion adsorption mechanisms. Selenite was observed to form inner-sphere surface complexes on the Fe oxides: goethite, amorphous Fe oxide (Hayes et al., 1987; Manceau and Charlet, 1994), hematite (Catalano et al., 2006), and maghemite (Jordan et al., 2014) using a range of spectroscopies. Extended X-ray absorption fine structure (EXAFS) results indicated a mixture of inner-sphere and outer-sphere Se(IV) surface complexes on amorphous Al oxide (Peak, 2006). Results for Se(VI) adsorption are more diverse, varying with mineral type and spectroscopic technique. Some EXAFS spectroscopy investigations found exclusively inner-sphere Se(VI) surface complexes on the Fe oxides: goethite, amorphous Fe oxide (Manceau and Charlet, 1994), hematite (Peak and Sparks, 2002), and maghemite (Das et al., 2013), whereas other EXAFS studies provided evidence for the formation of mixtures of inner-sphere and outer-sphere Se(VI) surface complexes on goethite, amorphous Fe oxide (Peak and Sparks, 2002), maghemite (Jordan et al., 2013), and amorphous Al oxide (Peak, 2006). The surface configuration of Se(VI) on maghemite was found to be outer-sphere, as observed with attenuated total reflectance–Fourier transform infrared spectroscopy (Jordan et al., 2013). The type of Se(VI) surface complex observed on goethite with attenuated total reflectance–Fourier transform infrared was predominantly inner-sphere at solution pH values less than 6 and predominantly outer-sphere at pHs higher than 6 (Wijnja and Schulthess, 2000).

In summary, macroscopic and microscopic experimental evidence on various oxide minerals indicates strong specific adsorption of Se(IV) forming predominantly inner-sphere surface complexes. Selenate adsorption exhibits evidence for varying proportions of inner-sphere and outer-sphere surface complexation, dependent on the adsorbent mineral. Formation of weaker outer-sphere Se(VI) surface complexes is also consistent with the reduced amount of Se(VI) adsorption compared with Se(IV) adsorption observed in soils.

Selenium adsorption on soils and soil minerals has been described using various surface complexation models. For Se(IV), these include the constant capacitance model (Sposito et al., 1988; Goldberg and Glaubig, 1988; Anderson and Benjamin, 1990a, 1990b; Duc et al., 2003, 2006; Goldberg et al., 2007, 2008a; Goldberg, 1985; Gabos et al., 2014), the diffuse layer model (Dzombak and Morel, 1990; Balistrieri et al., 2003; Jordan et al., 2009a, 2009b; Kim et al., 2012), the triple layer model (Benjamin and Bloom, 1981; Hayes et al., 1988; Balistrieri and Chao, 1990; Zhang and Sparks, 1990; Ghosh et al., 1994; Wu et al., 2000; Martinez et al., 2006; Rovira et al., 2008; Goldberg, 2013, 2014), and the CD-MUSIC model (Hiemstra and van Riemsdijk, 1999; Hiemstra et al., 2007). For Se(VI), model applications have also included the constant capacitance model (Goldberg et al., 2008a; Gabos et al., 2014), the diffuse layer model (Dzombak and Morel, 1990), the triple layer model (Davis and Leckie, 1980; Benjamin and Bloom, 1981; Hayes et al., 1988; Balistrieri and Chao, 1990; Ghosh et al., 1994; Wu et al., 2000, 2001; Martinez et al., 2006; Rovira et al., 2008; Goldberg, 2014), and the CD-MUSIC model (Rietra et al., 2001; Perez et al., 2014).

Selenate adsorption by 15 diverse soils from the United States (Goldberg et al., 2008a) and 15 tropical soils from Brazil (Gabos et al., 2014) had been described using the constant capacitance model. This model assumes that all adsorbing ions form inner-sphere surface complexes. Goldberg et al. (2008a) used one monodentate surface complex and Gabos et al. (2014) used two monodentate surface complexes to describe their Se(VI) adsorption data. Perez et al. (2014) were well able to describe Se (VI) adsorption by two ferralic soils from Brazil high in iron oxides with the CD-MUSIC model. Their optimizations indicated monodentate Se(VI) surface complexes that were primarily outer-sphere but included a small portion of inner-sphere Se (VI) surface species.

Traditionally, surface complexation models have been implemented using either exclusively inner-sphere or outer-sphere surface configurations. Recent triple layer model applications have successfully used a combination of inner-sphere and outer-sphere surface complexes to describe Se(IV) adsorption by soils, clay minerals, amorphous oxides (Goldberg, 2013), and gibbsite as well as Se(VI) adsorption by gibbsite (Goldberg, 2014) and a Brazilian ferralsol (Perez et al., 2014). Given that both Se(IV) and Se(VI) were found to adsorb as mixtures of inner-sphere and outer-sphere surface complexes on some of the reference minerals, it is appropriate that both of these surface configurations be included in model applications describing adsorption of these ions by soils.

The objectives of the present study were (i) to determine Se (VI) adsorption on a variety of soils as a function of solution pH and (ii) to evaluate for the first time the ability of the triple layer model to describe Se(VI) adsorption on these soils using both inner-sphere and outer-sphere surface configurations.

MATERIALS AND METHODS

Selenate adsorption was investigated on a variety of adsorbents. Amorphous Al and Fe oxides were synthesized using the method of Sims and Bingham (1968). X-ray diffraction (XRD) analyses of powder mounts found no detectable crystalline impurities and verified that the materials were amorphous. Samples of kaolinite (KGa-1b, well-crystallized Georgia kaolinite, and KGa-2, poorly crystallized Georgia kaolinite), Na-montmorillonite (SWy-1, Wyoming bentonite), Ca-montmorillonite (SAz-1, Cheto montmorillonite), and IMt-2 illite (Silver Hill illite) were purchased from the Clay Minerals Society's Source Clay Repository (Purdue University, West Lafayette, IN). The montmorillonites and kaolinites were used without any pretreatment. The illite sample was ground to pass through a 0.05-mm sieve using a mortar and pestle. Trace impurities found with XRD analyses of powder mounts were vermiculite and feldspar in the KGa-1b kaolinite, chlorite in the KGa-2 kaolinite, mica in the SWy-1 montmorillonite, and vermiculite in the IMt-1 illite. No impurities were found in the SAz-1 montmorillonite using XRD. Surface areas determined from single-point BET N_2 adsorption isotherms are 25.6 $m^2\ g^{-1}$ for amorphous Al oxide, 158 $m^2\ g^{-1}$ for amorphous Fe oxide, 10.1 $m^2\ g^{-1}$ for KGa-1b kaolinite, 20.8 $m^2\ g^{-1}$ for KGa-2 kaolinite, 24.8 $m^2\ g^{-1}$ for SWy-1 montmorillonite, 68.9 $m^2\ g^{-1}$ for SAz-1 montmorillonite, and 23.1 $m^2\ g^{-1}$ for illite.

Selenate adsorption was investigated using soil samples belonging to 18 different soil series. These soils were selected from the set of Southwestern and Midwestern US soil samples investigated by Goldberg et al. (2007) because they had adsorbed significant amounts of Se(IV). The soils also covered a range of chemical characteristics as indicated in Table 1. Nohili soil was obtained from the island of Kauai, Hawaii. The Panhill and the Panoche soils were included because they had been previously investigated for Se(VI) adsorption on alluvial California soils by Neal and Sposito (1989). Detailed descriptions of the analytical methods used to characterize the soil samples are provided in Goldberg et al. (2007). Briefly, cation exchange capacity was measured according to the arid zone soil method of Rhoades (1982), surface area was determined by the ethylene glycol monoethyl ether adsorption method of Cihacek and Bremner (1979), and free Fe and Al oxides were determined using a citrate/citric acid buffer and hydrosulfite (Coffin, 1963). A carbon coulometer was used to determine total carbon by furnace combustion, inorganic carbon

TABLE 1. Classifications and Chemical Characteristics of Soils†

Soil Series	Depth	pH	CEC	SA	IOC	OC	Fe	Al
	cm		$mmol_c\ kg^{-1}$	$km^2\ kg^{-1}$	$g\ kg^{-1}$	$g\ kg^{-1}$	$g\ kg^{-1}$	$g\ kg^{-1}$
Fiander (fine-silty, mixed, mesic Typic Natraquoll)	0–15	9.60	248	0.0925	6.9	4.0	9.2	1.06
Nohili (very-fine, smectitic, calcareous, isohyperthermic Cumulic Endoaquoll)	0–23	8.01	467	0.286	2.7	21.3	49.0	3.7
Panhill (fine-silty, mixed, superactive, thermic Mollic Haplargid)	0–15	8.79	108	0.0336	2.5‡	5.8‡	3.4	0.29
Panoche (fine-loamy, mixed, superactive, thermic Typic Haplocambid)	0–15	8.10	186	0.0768	4.2‡	5.6‡	4.1	0.37
Porterville (fine, smectitic, thermic Aridic Haploxerert)	0–7.6	6.76	203	0.137	0.039	9.4	10.7	0.90
Wyo (fine-loamy, mixed, thermic Mollic Haploxeralf)		6.37	155	0.0539	0.014	19.9	9.5	0.89
Yolo (fine-silty, mixed, nonacid, thermic Typic Xerorthent)	0–15	8.43	177	0.0730	0.23	11.5	15.6	1.13
Bernow (fine-loamy, siliceous, thermic Glossic Paleudalf)	B	3.87	77.6	0.0464	0.0028	3.8	8.1	1.1
Canisteo (fine-loamy, mixed, superactive, calcareous, mesic Typic Endoaquoll)	A	7.99	195	0.152	14.8	34.3	1.7	0.44
Dennis (fine, mixed, thermic Aquic Argiudoll)	B	5.29	63.1	0.0724	0.0010	5.2	30.0	4.1
Hanlon (coarse-loamy, mixed, superactive, mesic Cumulic Hapludoll)	A	7.56	142	0.0587	2.6	15.1	3.7	0.45
Kirkland (fine, mixed, superactive, thermic Udertic Paleustoll)	A	5.02	154	0.0421	0.014	12.3	5.6	0.80
Osage (fine, smectitic, thermic Typic Epiaquert)	B	6.43	384	0.143	0.0100	18.9	16.5	1.3
Pond Creek (fine-silty, mixed, superactive, thermic Pachic Argiustoll)	B	6.15	106	0.0596	0.016	5.0	5.1	0.81
Pratt (sandy, mixed, mesic Lamellic Haplustalf)	B	5.74	23.3	0.117	0.0007	2.1	0.92	0.13
Richfield (fine, smectitic, mesic Aridic Argiustoll)	B	7.38	275	0.082	0.040	8.0	5.4	0.76
Summit (fine, smectitic, thermic Oxyaquic Vertic Argiudoll)	A	7.46	374	0.218	0.25	26.7	16.2	2.3
Taloka (fine, mixed, thermic Mollic Albaqualf)	A	4.90	47.4	0.087	0.0021	9.3	3.6	0.62

†Excerpted from Goldberg et al. (2007).
‡From Martens and Suarez (1997).

(IOC) by acidification and heating, and organic carbon (OC) by the difference between total carbon and IOC.

Selenate adsorption envelopes (amount of Se(VI) adsorbed as a function of solution pH per fixed total Se(VI) concentration) were determined in batch systems. Samples of solid (0.1 g for oxides, 1.0 g for soils, and 1.2 g for clays) were equilibrated with aliquots (200 mL for Fe oxide, 100 mL for Al oxide, 30 mL for clays, and 25 mL for soils) of a 0.1-*M* NaCl background electrolyte solution on a reciprocating shaker. The background electrolyte solution also contained 20 μmol Se(VI) L^{-1} and had been adjusted to the desired pH values (2–10) using 1 *M* HCl or 1 *M* NaOH. After 2 h of reaction time, the samples were centrifuged and decanted. The solutions were analyzed for pH, filtered using 0.45-μm membrane filters, and analyzed for Se concentration using an inductively coupled plasma optical emission spectrometer.

The theory and assumptions of the triple layer model are discussed in detail in Davis and Kent (1990) and Goldberg (1992). The protonation, dissociation, and background electrolyte surface complexation reactions are:

$$SOH_{(s)} + H^+_{(aq)} \leftrightarrow SOH^+_{2(s)} \quad (1)$$

$$SOH_{(s)} \leftrightarrow SO^-_{(s)} + H^+_{(aq)} \quad (2)$$

$$SOH_{(s)} + Na^+_{(aq)} \leftrightarrow SO^- - Na^+_{(s)} + H^+_{(aq)} \quad (3)$$

$$SOH_{(s)} + H^+_{(aq)} + Cl^-_{(aq)} \leftrightarrow SOH^+_2 - Cl^-_{(s)} \quad (4)$$

where $SOH_{(s)}$ represents a reactive surface functional group: either a hydroxyl on oxide minerals or an aluminol on clay mineral edges.

The current study evaluates the use of a combination of inner-sphere and outer-sphere surface complexes in the triple layer model to describe Se(VI) adsorption by oxides, clays, and soils. This approach has previously provided excellent fits to Se (VI) adsorption by gibbsite (Goldberg, 2014). In the current model application, the following Se(VI) surface complexation reactions are considered:

$$SOH_{(s)} + HSeO^-_{4(aq)} + H^+_{(aq)} \leftrightarrow SHSeO_{4(s)} + H_2O \quad (5)$$

$$SOH_{(s)} + HSeO^-_{4(aq)} \leftrightarrow SSeO^-_{4(s)} + H_2O \quad (6)$$

$$SOH_{(s)} + HSeO^-_{4(aq)} + H^+_{(aq)} \leftrightarrow SOH^+_2 - HSeO^-_{4(s)} \quad (7)$$

$$SOH_{(s)} + HSeO^-_{4(aq)} \leftrightarrow SOH^+_2 - SeO^{2-}_{4(s)} \quad (8)$$

Surface complexation constants for reactions (1) to (8) are:

$$K_+(\text{int}) = \frac{[SOH^+_2]}{[SOH][H^+]} \exp(F\psi_o/RT) \quad (9)$$

$$K_-(int) = \frac{[SO^-][H^+]}{[SOH]} \exp(-F\psi_o/RT) \quad (10)$$

$$K_{Na^+}(\text{int}) = \frac{[SO^- - Na^+][H^+]}{[SOH][Na^+]} \exp\left[F\left(\psi_\beta - \psi_o\right)/RT\right] \quad (11)$$

$$K_{Cl^-}(\text{int}) = \frac{[SOH^+_2 - Cl^-]}{[SOH][H^+][Cl^-]} \exp\left[F\left(\psi_o - \psi_\beta\right)/RT\right] \quad (12)$$

$$K_{Se}^{1is}(\text{int})=\frac{[SHSeO_4]}{[SOH][HSeO_4^-][H^+]} \quad (13)$$

$$K_{Se}^{2is}(\text{int})=\frac{[SSeO_4^-]}{[SOH][HSeO_4^-]}\exp(-F\psi_o/RT) \quad (14)$$

$$K_{Se}^{1os}(\text{int})=\frac{[SOH_2^+-HSeO_4^-]}{[SOH][HSeO_4^-][H^+]}\exp[F(\psi_o-\psi_\beta)/RT] \quad (15)$$

$$K_{Se}^{2os}(\text{int})=\frac{[SOH_2^+-SeO_4^{2-}]}{[SOH][HSeO_4^-]}\exp[F(\psi_o-2\psi_\beta)/RT] \quad (16)$$

where square brackets represent concentrations (mol L^{-1}), F is the Faraday constant (C mol_c^{-1}), ψ_o is the surface potential (V) in the o-plane of inner-sphere (is) adsorption, ψ_β is the surface potential (V) in the β-plane of outer-sphere (os) adsorption, R is the molar gas constant (J mol^{-1} K^{-1}), and T is the absolute temperature (K). The electrostatic potential, $e^{-F\psi/RT}$, terms can be considered as solid-phase activity coefficients correcting for charge on the surface complexes in each plane of adsorption. It has been shown by Sposito (1983) that surface complexation models can be considered as special cases of the van der Waals model in statistical mechanics. Charged surface complexes interact mutually to create a long-range mean electric force field arising from screened coulombic forces, whereas short-range interactions are neglected. The electrostatic potential terms in the equilibrium constant expressions represent contributions of the mean electric force field to the solid-phase activity coefficients (Sposito, 1983).

The charge balance equations are:

$$\sigma_o+\sigma_\beta+\sigma_d=0 \quad (17)$$

$$\sigma_o=[SOH_2^+]+[SOH_2^+-Cl^-]-[SSeO_4^-]+[SOH_2^+-HSeO_4^-]+[SOH_2^+-SeO_4^{2-}]-[SO^-]-[SO^--Na^+] \quad (18)$$

$$\sigma_\beta=[SO^--Na^+]-[SOH_2^+-Cl^-]-[SOH_2^+-HSeO_4^-]-2[SOH_2^+-SeO_4^{2-}] \quad (19)$$

$$\sigma_d=\frac{S_A C_s}{F}(8\varepsilon_0 DRTI)^{1/2}\sinh(F\psi_d/RT) \quad (20)$$

where ε_0 is the permittivity of vacuum, D is the dielectric constant of water, I is the ionic strength, S_A is the surface area (m^2 g^{-1}), C_s is the solid concentration (g L^{-1}), ψ_d is the surface potential (V) in the d-plane of the diffuse ion swarm, and the surface charges σ_i have units (mol_c L^{-1}). The mass balance equation for the reactive surface functional group is:

$$SOH_T=[SOH]+[SOH_2^+]+[SO^-]+[SO^--Na^+]+[SOH_2^+-Cl^-]+[SHSeO_4]+[SSeO_4^-]+[SOH_2^+-HSeO_4^-]+[SOH_2^+-SeO_4^{2-}] \quad (21)$$

where SOH_T, the total number of reactive surface functional groups (mol L^{-1}), is related to the surface site density, N_s (sites nm^{-2}):

$$SOH_T=\frac{S_A C_s 10^{18}}{N_A}N_s \quad (22)$$

where N_A is the Avogadro number.

Initial input parameter values for the triple layer model were surface area, surface site density: N_S = 2.31 sites nm^{-2} (recommended for natural materials by Davis and Kent, 1990); capacitances: C_1 = 1.2 F m^{-2}, C_2 = 0.2 F m^{-2} (considered optimum by Zhang and Sparks, 1990); protonation constant: $\log K_+(\text{int})$ = 4.3; dissociation constant: $\log K_-(\text{int})$ = −9.8; background electrolyte constants: $\log K_{Na+}(\text{int})$ = − 9.3, $\log K_{Cl-}(\text{int})$ = 5.4 (from Zhang and Sparks, 1990) for Fe oxide; protonation constant: $\log K_+(\text{int})$ = 5.0; dissociation constant: $\log K_-(\text{int})$ = −11.2; background electrolyte constants: $\log K_{Na+}(\text{int})$ = −8.6, $\log K_{Cl-}(\text{int})$ = 7.5 (from Sprycha, 1989a, 1989b) for amorphous Al oxide, clay minerals, and soils. These sets of parameter values had been used in a prior application of the triple layer model to Se(IV) adsorption by oxides, clay minerals, and soils (Goldberg, 2013).

The computer code FITEQL 4.0 (Herbelin and Westall, 1999) was used to fit Se(VI) surface complexation constants to the experimental adsorption data. This computer program uses a nonlinear least-squares optimization routine to fit equilibrium constants to adsorption data and contains the triple layer model. Goodness-of-fit was evaluated using the overall variance parameter V_Y:

$$V_Y=\frac{SOS}{DF} \quad (23)$$

where SOS is the weighted sum of squares of the residuals, and DF is the degrees of freedom. Values of $V_Y < 10$ are considered a good fit of the model to the data (Herbelin and Westall, 1999).

RESULTS AND DISCUSSION

Selenate adsorption as a function of solution pH is presented in Fig. 1 for amorphous Al and Fe oxides and the clay minerals kaolinite and illite. For the amorphous Al oxide (Fig. 1A), Se (VI) adsorption exhibited a broad maximum up to pH 7 and then decreased with increasing solution pH. Somewhat similar pH-dependent behavior had been observed previously for Se(IV) adsorption by the same amorphous Al oxide. However, the adsorption maximum extended up to pH 8 (Goldberg, 2013). These results agree with those on gibbsite where the adsorption maximum for Se(IV) adsorption extended to a higher pH than for Se (VI) adsorption (Goldberg, 2014). Selenate adsorption on the amorphous Fe oxide (Fig. 1B) exhibited a maximum in the pH range 2 to 4, a rapid decrease from pH 6 to 7.5, and minimal adsorption above pH 8.5. This behavior was in contrast to that for Se(IV) adsorption on the same amorphous Fe oxide, where a broad maximum was observed up to pH 8 (Goldberg, 2013). For both oxides, the amount of Se(VI) adsorption was approximately half the amount of Se(IV) adsorption, consistent with previous literature findings that Se(VI) adsorbs less than Se(IV) (Balistrieri and Chao, 1987; Duc et al., 2003).

Selenate adsorption on the clay minerals presented as a continuously decreasing function of increasing solution pH, with minimal adsorption above pH 8 for kaolinite (Fig. 1C presents results for KGa-1b kaolinite) and above pH 3 for illite (Fig. 1D). No adsorption maxima were found for Se(VI), in contrast to the adsorption peaks exhibited by Se(IV) on these clay minerals in the solution pH range 4 to 5 (Goldberg, 2013). As was the case for the oxides, the amount of Se(VI) adsorption on kaolinite and illite clay was much less than the amount of Se(IV) adsorption that had been observed previously (Goldberg, 2013). The increased adsorption on kaolinite over illite is most likely caused by the greater proportion of edge charge found on kaolinite. No Se(VI) adsorption was found on either of the two montmorillonites investigated.

The ability of the triple layer model to describe Se(VI) adsorption on the oxides and clay minerals is presented in Fig. 1.

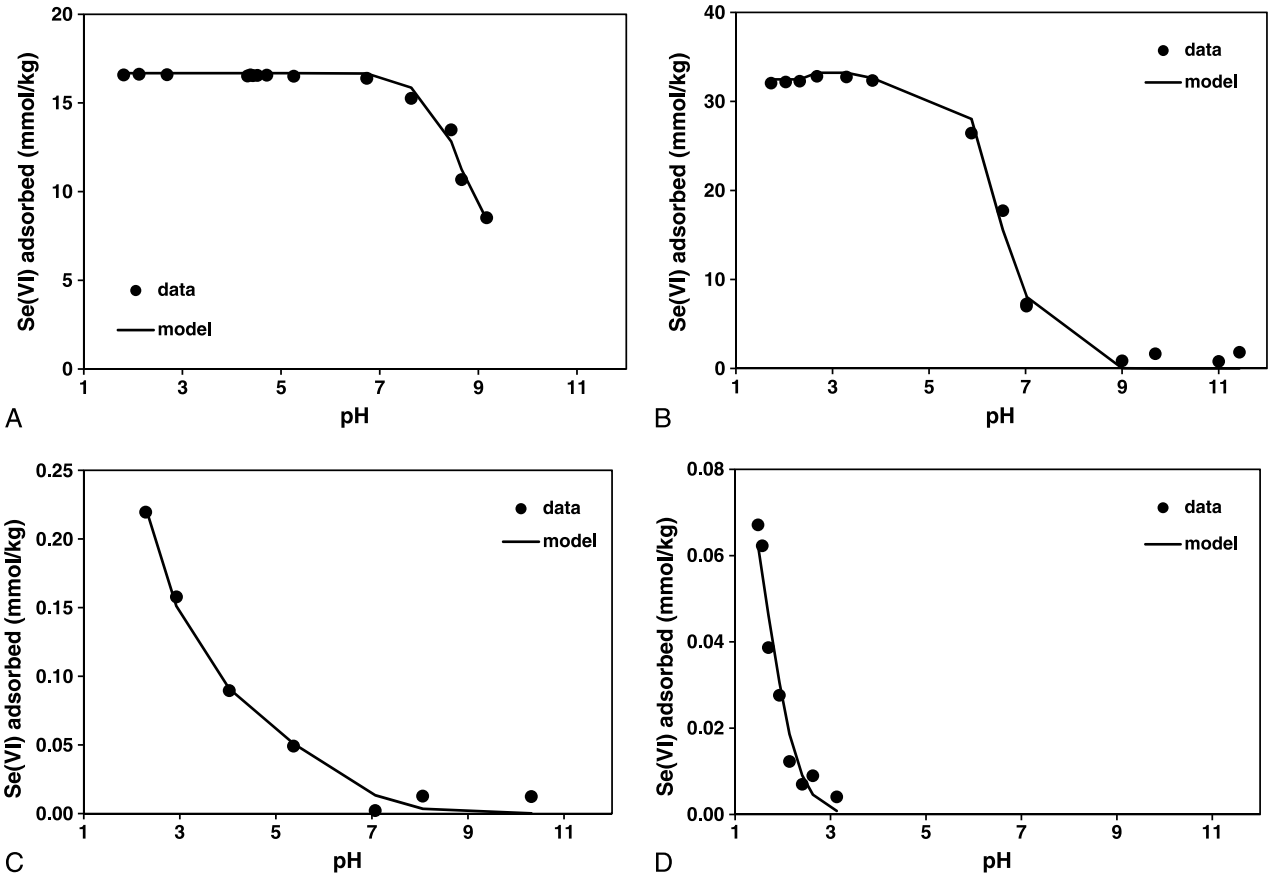

FIG. 1. Fit of the triple layer model to Se(VI) adsorption on oxides and clay minerals: (A) amorphous Al oxide; (B) amorphous Fe oxide; (C) kaolinite; (D) illite. Experimental data are represented by circles. Model fits are represented by a solid line.

For all materials, the model was able to provide a quantitative description of the adsorption data over the entire pH range investigated as evidenced by the very low values of V_Y, the goodness-of-fit criterion presented in Table 2. Values of the optimized Se (VI) surface complexation constants for the oxides and clays are provided in Table 2. The Se(VI) surface speciations obtained with the triple layer model for the amorphous oxides are presented in Fig. 2. For the amorphous Fe oxide, the inner-sphere surface complex predominates until the solution pH reaches 10 (Fig. 2A). This finding is in agreement with the spectroscopic results of Peak and Sparks (2002) who observed a mixture of inner-sphere and outer-sphere Se(VI) surface complexes on amorphous Fe oxide. Two outer-sphere Se(VI) surface complexes were required to describe adsorption on the amorphous Al oxide (Fig 2B). The propensity to form outer-sphere anion surface complexes on amorphous Al oxide has been observed previously for molybdate (Goldberg et al., 2008b) and selenite (Goldberg, 2013), indicating weaker adsorption than on amorphous Fe oxide where inner-sphere anion surface complexes predominate. This result is in agreement with the spectroscopic results of Peak (2006) who observed predominantly outer-sphere surface complexes on amorphous Al oxide.

The triple layer model was able to describe Se(VI) adsorption on both kaolinites using two outer-sphere surface complexes (Fig. 1C shows results for KGa-1b kaolinite) and on illite using one inner-sphere surface complex (Fig. 1D). Spillover of permanent negative charge from the interlayers (Secor and Radke, 1985) may be responsible for reducing the adsorption of negatively charged selenate by the 2:1 layer clay mineral illite compared with adsorption by the 1:1 layer clay mineral kaolinite. Previous triple layer modeling of Se(IV) adsorption by clays had included an inner-sphere surface complex on illite but not on kaolinite, suggesting

TABLE 2. Triple Layer Model Se(VI) Surface Complexation Constants

Solid	$LogK^{2is}_{Se(VI)}$	$LogK^{1os}_{Se(VI)}$	$LogK^{2os}_{Se(VI)}$	V_Y
Oxides				
Amorphous Al oxide		19.6	13.2	0.06
Amorphous Fe oxide	8.54		6.47	0.3
Clay minerals				
KGa-1b kaolinite		9.82	6.86	0.1
KGa-2 kaolinite		8.95	6.44	1.3
IMt-2 illite	−2.13			0.05
Soils				
Nohili		8.35	4.67	0.6
Bernow B		9.06	5.87	0.2
Dennis B		10.4	6.39	0.6
Kirkland A		8.13	5.44	0.6
Osage B		8.26	4.80	0.2
Pond Creek B	−4.30		6.54	0.2
Pratt B	−5.60		6.40	6.0
Richfield B		7.43	4.28	0.0006
Summit A		8.35	4.54	0.02
Soil average logK(int)	−4.95 ± 0.92	8.57 ± 0.94	5.44 ± 0.89	

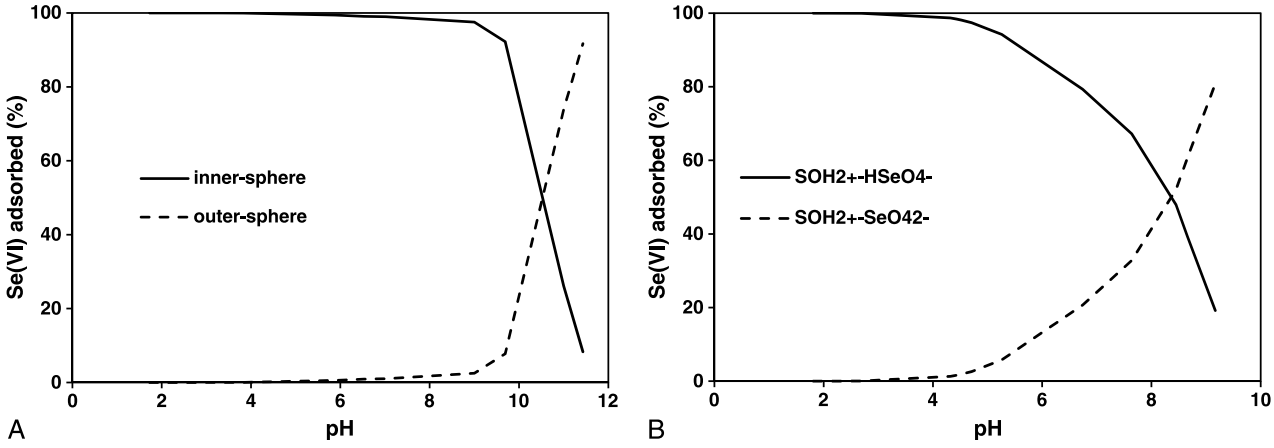

FIG. 2. Surface speciation predicted by the triple layer model for Se(VI) adsorption on oxides: (A) amorphous Fe oxide; (B) amorphous Al oxide.

slightly stronger adsorption by illite (Goldberg, 2013). The model result indicating inner-sphere adsorption of Se(VI) on illite suggests that, despite its lower amount of total adsorption, Se(VI) may be adsorbed more strongly than on kaolinites where model results indicated outer-sphere surface complexes. Clearly, spectroscopic experiments of Se(VI) and Se(IV) adsorption are needed to provide direct determination of Se surface configurations and adsorption mechanisms on these clay minerals.

Selenate adsorption as a function of solution pH was not observed on any of the six Southwestern soils investigated. A previous investigation by Neal and Sposito (1989) of the Panhill and Panoche soils had also failed to find Se(VI) adsorption. These researchers had carried out their study under CO_2-free air, which would have greatly increased aqueous calcium concentrations in these calcareous soils. Three of the Midwestern soils also showed no Se(VI) adsorption. Figure 3 depicts Se(VI) adsorption for the

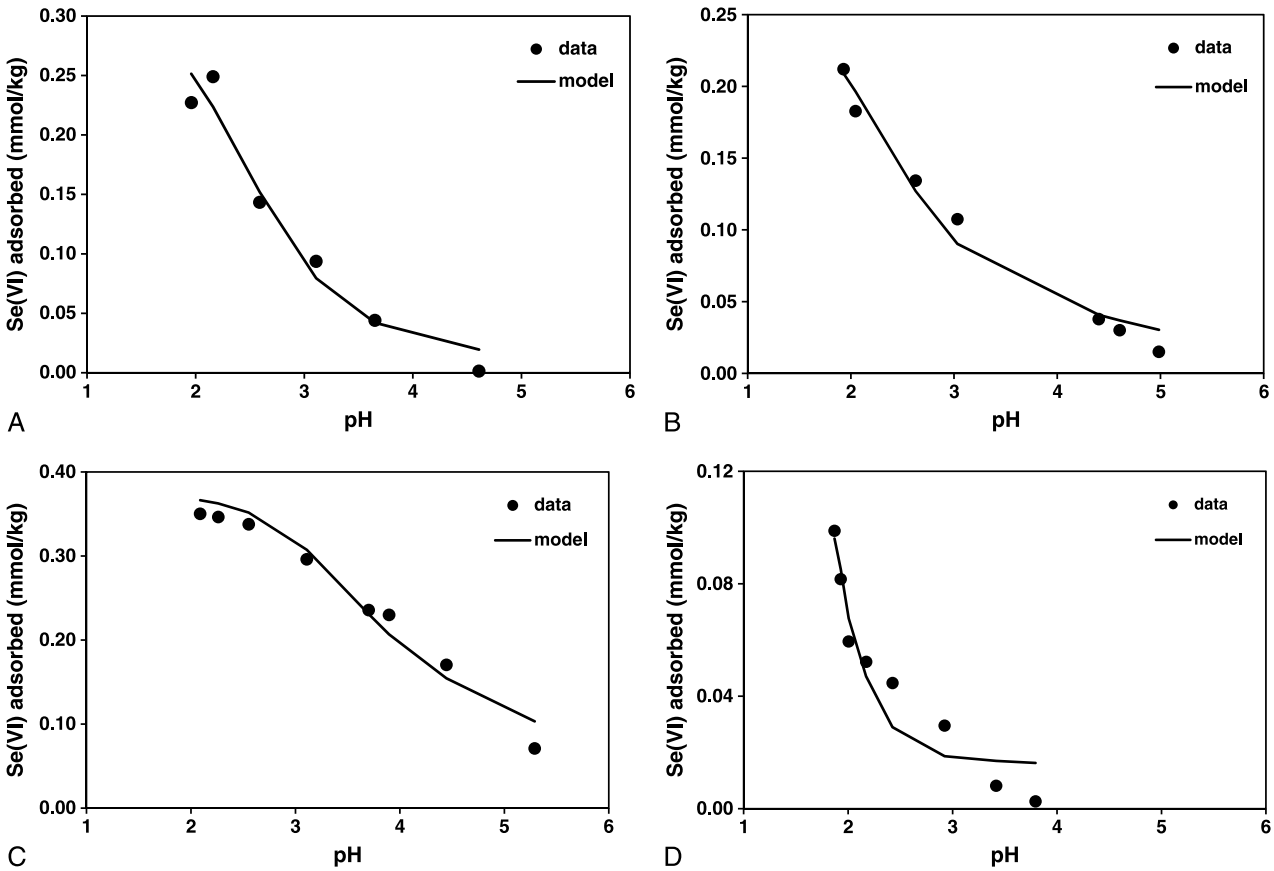

FIG. 3. Fit of the triple layer model to Se(VI) adsorption on soils: (A) Nohili soil; (B) Bernow soil; (C) Dennis soil; (D) Pond Creek soil. Experimental data are represented by circles. Model fits are represented by a solid line.

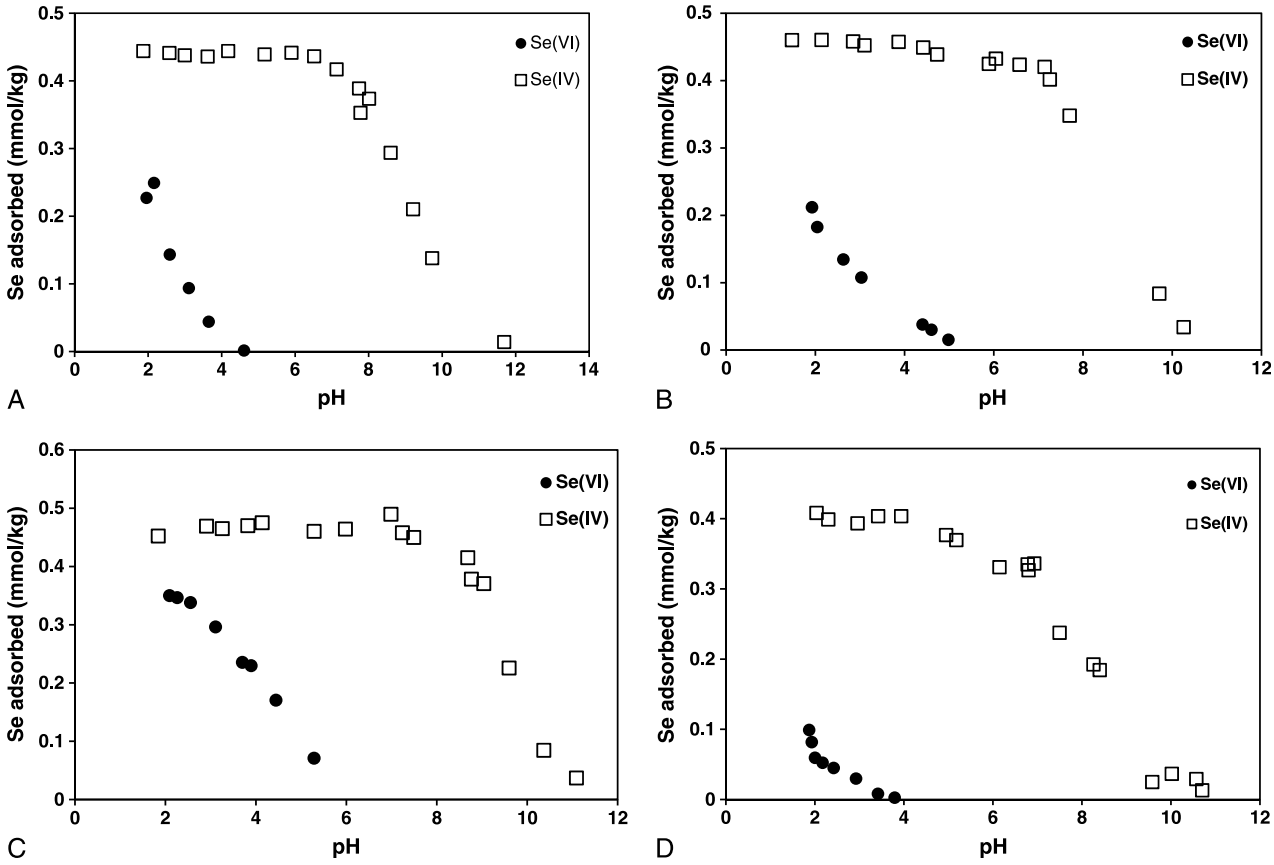

FIG. 4. Comparison of Se(VI) and Se(IV) adsorption on soils: (A) Nohili soil; (B) Bernow soil; (C) Dennis soil; and (D) Pond Creek soil. Selenate data are represented by circles. Selenite data are represented by squares.

Nohili soil from Kauai, Hawaii (Fig. 3A) and three Midwestern soils (Fig. 3B–D). Selenate adsorption was only found at acid pH and decreased rapidly with increasing solution pH. The decrease in adsorption commenced at a much lower solution pH value for Se(VI) than had been found previously for Se(IV) adsorption by the soils (Goldberg et al., 2007). In addition, the magnitude of Se(VI) adsorption was much less than for Se(IV) adsorption by these soils (Fig. 4). Comparison of the chemical properties of the soils that adsorbed Se(VI) as opposed to those that did not indicated higher Fe and Al oxide contents, lower inorganic carbon content, and higher cation exchange capacity. However, none of these differences were statistically significant between the two groups of soils.

The ability of the triple layer model to describe Se(VI) adsorption by the Hawaiian soil and three Midwestern soils is depicted in Fig. 3. The model provided a quantitative description of the adsorption data on the soils (Fig. 3), with the exception of some underprediction between pH 2 to 3 and some overprediction between pH 3 to 4 for the Pond Creek soil (Fig. 3D). Optimized values of Se(VI) surface complexation constants for the soils are listed in Table 2, which also shows low values for the goodness-of-fit criterion. A representative Se(VI) surface speciation obtained with the triple layer model for one of the soils is presented in Fig. 5. Two outer-sphere surface complexes were used to describe the Se(VI) adsorption data, which is consistent with the weak adsorption behavior of Se(VI) on soils and soil minerals. The results are also consistent with those of Perez et al. (2014) who obtained predominantly outer-sphere surface complexes when fitting the CD-MUSIC model to Se(VI) adsorption by two Brazilian soils. A prior application of the triple layer model to describe Se(IV) adsorption on the soils used in the current study had included an inner-sphere surface complex along with the outer-sphere surface complexes (Goldberg, 2013)—evidence of the greater strength of adsorption exhibited by Se(IV) species over Se(VI) species.

Results of the current study agree with previous literature findings for Se adsorption by oxides, clay minerals, and soils. The extent of Se(VI) adsorption by these materials was less than

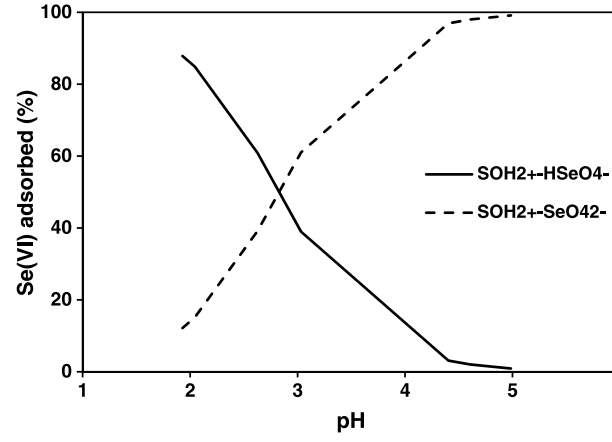

FIG. 5. Surface speciation predicted by the triple layer model for Se (VI) adsorption on Bernow soil.

that of Se(IV) adsorption. In addition, significant adsorption of Se (VI) was restricted to the acid pH range, especially on clays and soils. Selenate adsorption was not found on Southwestern soils likely because of their low Fe and Al oxide contents. The triple layer model was well able to describe Se(VI) adsorption on oxides, clay minerals, and soils. Selenate surface species were predominantly outer-sphere complexes, consistent with the weak adsorption of Se(VI) compared with the more strongly adsorbing Se(IV) species where inner-sphere surface complexes were significant. The low amount of Se(VI) adsorption must be considered in the management of Se, especially in oxidizing environments where Se(VI) is the thermodynamically stable and usually predominant species. In soil environments where Se(IV) coexists with Se(VI), adsorption of Se(VI) would also be reduced by competition from the more strongly adsorbing Se(IV) species. From a health standpoint, it is fortunate that the more poorly adsorbing Se species, Se(VI), is the less toxic redox state.

ACKNOWLDEGMENTS

The author thanks Ms. P. Xiong and Mr. A. Rios for technical assistance.

REFERENCES

Adriano D. C. 2001. Trace Elements in Terrestrial Environments. Biogeochemistry, Bioavailability, and Risks of Metals. Springer-Verlag, New York, NY.

Anderson P. R., and M. M. Benjamin. 1990a. Constant capacitance surface complexation model. Adsorption in silica-iron binary oxide suspensions. Am. Chem. Soc. Symp. Ser. 416:272–281.

Anderson P. R., and M. M. Benjamin. 1990b. Modeling adsorption in aluminum—Iron binary oxide suspensions. Environ. Sci. Technol. 24: 1586–1592.

Balistrieri L. S., and T. T. Chao. 1987. Selenium adsorption by goethite. Soil Sci. Soc. Am. J. 51:1145–1151.

Balistrieri L. S., and T. T. Chao. 1990. Adsorption of selenium by amorphous iron oxyhydroxide and manganese dioxide. Geochim. Cosmochim. Acta. 54:739–751.

Balistrieri L. S., S. E. Box, and J. W. Tonkin. 2003. Modeling precipitation and sorption of elements during mixing of river water and porewater in the Coeur d'Alene River basin. Environ. Sci. Technol. 37:4694–4701.

Benjamin M. M., and N. S. Bloom. 1981. Effects of strong binding of anionic adsorbates on adsorption of trace metals on amorphous iron oxyhydroxide. *In*: Adsorption From Aqueous Solutions. Tewari P. H. (ed.). Plenum Publishing Corporation, New York, NY, pp. 41–60.

Catalano J. G., Z. Zhang, P. Fenter, and M. J. Bedzyk. 2006. Inner-sphere adsorption geometry of Se(IV) at the hematite (100)-water interface. J. Colloid Interface Sci. 297:665–671.

Cihacek L. J., and J. M. Bremner. 1979. A simplified ethylene glycol monoethyl ether procedure for assessing soil surface area. Soil Sci. Soc. Am. J. 43:821–822.

Coffin D. E.. 1963. A method for the determination of free iron oxide in soils and clays. Can. J. Soil Sci. 43:7–17.

Das S., M. J. Hendry, and J. Essilfie-Dughan. 2013. Adsorption of selenate onto ferrihydrite, goethite, and lepidocrocite under neutral pH conditions. Appl. Geochem. 28:185–193.

Davis J. A., and D. B. Kent. 1990. Surface complexation modeling in aqueous geochemistry. Rev. Mineral. 23:117–260.

Davis J. A., and J. O. Leckie. 1980. Surface ionization and complexation at the oxide/water interface. 3. Adsorption of anions. J. Colloid Interface Sci. 74:32–43.

Duc M., G. Lefevre, M. Fedoroff, J. Jeanjean, J. C. Ruchard, F. Monteil-Rivera, J. Dumenceau, and S. Milonjic. 2003. Sorption of selenium anionic species on apatites and iron oxides from aqueous solutions. J. Environ. Radioact. 70:61–72.

Duc M., G. Lefevre, and M. Fedoroff. 2006. Sorption of selenite ions on hematite. J. Colloid Interface Sci. 298:556–563.

Dzombak D. A., and F. M. M. Morel. 1990. Surface Complexation Modeling: Hydrous Ferric Oxide. New York, NY, John Wiley.

Fernandez C. M. G., M. A. Palacios, and C. Camara. 1993. Flow-injection and continuous-flow systems for the determination of Se(IV) and Se(VI) by hydride generation atomic absorption spectrometry with on-line prereduction of Se(VI) to Se(IV). Anal. Chim. Acta. 283:386–392.

Gabos M. B., S. Goldberg, and L. R. F. Alleoni. 2014. Modeling selenium (IV and VI) adsorption envelopes in selected tropical soils using the constant capacitance model. Environ. Toxicol. Chem. 33: 2197–2207.

Ghosh M. M., C. D. Cox, and J. R. Yuan-Pan. 1994. Adsorption of selenium on hydrous alumina. Environ. Progress. 13:79–88.

Girling C. A. 1984. Selenium in agriculture and the environment. Agric. Ecosyst. Environ. 11:37–65.

Goldberg S. 1985. Chemical modeling of anion competition on goethite using the constant capacitance model. Soil Sci. Soc. Am. J. 49:851–856.

Goldberg S. 1992. Use of surface complexation models in soil chemical systems. Adv. Agron. 47:233–329.

Goldberg S. 2013. Modeling selenite adsorption envelopes on oxides, clay minerals, and soils using the triple layer model. Soil Sci. Soc. Am. J. 77:64–71.

Goldberg S. 2014. Macroscopic experimental and modeling evaluation of selenite and selenate adsorption mechanisms on gibbsite. Soil Sci. Soc. Am. J. 78:473–479.

Goldberg S., and R. A. Glaubig. 1988. Anion sorption on a calcareous, montmorillonitic soil—Selenium. Soil Sci. Soc. Am. J. 52:954–958.

Goldberg S., S. M. Lesch, and D. L. Suarez. 2007. Predicting selenite adsorption by soils using soil chemical parameters in the constant capacitance model. Geochim. Cosmochim. Acta. 71:5750–5762.

Goldberg S., S. Hyun, and L. S. Lee. 2008a. Chemical modeling of arsenic (III, V) and selenium (IV, VI) adsorption by soils surrounding ash disposal facilities. Vadose Zone J. 7:1231–1238.

Goldberg S., C. T. Johnston, D. L. Suarez, and S. M. Lesch. 2008b. Mechanism of molybdenum adsorption on soils and soil minerals evaluated using vibrational spectroscopy and surface complexation modeling. In: Adsorption of metals by geomedia. II: Variables, mechanisms, and model applications. Developments in Earth and Environmental Sciences 7. M. O. Barnett, and Kent D. B. (eds.). Elsevier, Amsterdam, Netherlands, pp. 235–266.

Hansmann D. D., and M. A. Anderson. 1985. Using electrophoresis in modeling sulfate, selenite, and phosphate adsorption onto goethite. Environ. Sci. Technol. 19:544–551.

Hayes K. F., A. L. Roe, G. E. Brown, K. O. Hodgson, J. O. Leckie, and G. A. Parks. 1987. *In situ* X-ray absorption study of surface complexes: Selenium oxyanions on α-FeOOH. Science. 238:783–786.

Hayes K. F., C. Papelis, and J. O. Leckie. 1988. Modeling ionic strength effects on anion adsorption at hydrous oxide/solution interfaces. J. Colloid Interface Sci. 125:717–726.

Herbelin A. L., and J. C. Westall. 1999. FITEQL: A computer program for determination of chemical equilibrium constants from experimental data. Rep. 99-01, Version 4.0. Department of Chemistry, Oregon State University, Corvallis, OR.

Hiemstra T., and W. H. van Riemsdijk. 1999. Surface structural ion adsorption modeling of competitive binding of oxyanions by metal (hydr)oxides. J. Colloid Interface Sci. 210:182–193.

Hiemstra T., R. P. J. J. Rietra, and W. H. van Riemsdijk. 2007. Surface complexation of selenite on goethite: MO/DFT geometry and charge distribution. Croat. Chem. Acta. 80:313–324.

Jordan N., C. Lomenech, N. Marmier, E. Giffaut, and J.- J. Ehrhardt. 2009a. Sorption of selenium(IV) onto magnetite in the presence of silicic acid. J. Colloid Interface Sci. 329:17–23.

Jordan N., C. Lomenech, N. Marmier, E. Giffaut, and J.- J. Ehrhardt. 2009b. Competition between selenium(IV) and silicic acid on the hematite surface. Chemosphere. 75:129–134.

Jordan N., A. Ritter, H. Foerstendorf, A. C. Scheinost, S. Weiß, K. Heim, J. Grenzer, A. Mücklich, and H. Reuther. 2013. Adsorption mechanism of selenium(VI) onto maghemite. Geochim. Cosmochim. Acta. 103:63–75.

Jordan N., A. Ritter, A. C. Scheinost, S. Weiss, D. Schild, and R. Hübner. 2014. Selenium(IV) uptake by maghemite (γ-Fe_2O_3). Environ. Sci. Technol. 48:1665–1674.

Kim S. S., J. H. Min, J. K. Lee, M. H. Baik, J.- W. Choi, and H. S. Shin. 2012. Effects of pH and anions on the sorption of selenium ions onto magnetite. J. Environ. Radioact. 104:1–6.

Lakin H. W. 1961. Selenium Content of Soils. USDA-ARS Agriculture Handbook 200. U.S. Government Printing Office, Washington, DC. pp. 27–34.

Manceau A., and L. Charlet. 1994. The mechanism of selenate adsorption on goethite and hydrous ferric oxide. J. Colloid Interface Sci. 168:87–93.

Martens D. A., and D. L. Suarez. 1997. Selenium speciation of soil/sediment determined with sequential extractions and hydride generation atomic absorption spectrometry. Environ. Sci. Technol. 31:133–139.

Martinez M., J. Gimenez, J. de Pablo, M. Rovira, and L. Duro. 2006. Sorption of selenium(IV) and selenium(VI) onto magnetite. Appl. Surf. Sci. 252:3767–3773.

Masscheleyn P. H., R. D. Delaune, and W. H. Patrick. 1990. Transformations of selenium as affected by sediment oxidation-reduction potential and pH. Environ. Sci. Technol. 24:91–96.

Neal R. H., and G. Sposito. 1989. Selenate adsorption on alluvial soils. Soil Sci. Soc. Am. J. 53:70–74.

Ohlendorf H. M., D. J. Hoffman, M. K. Saiki, and T. W. Aldrich. 1986. Embryonic mortality and abnormalities of aquatic birds: Apparent impacts of selenium from irrigation drainwater. Sci. Total Environ. 52:49–63.

Peak D. 2006. Adsorption mechanisms of selenium oxyanion ions at the aluminum oxide/water interface. J. Colloid Interface Sci. 303:337–345.

Peak D., and D. L. Sparks. 2002. Mechanisms of selenate adsorption on iron oxides and hydroxides. Environ. Sci. Technol. 36:1460–1466.

Perez C., J. Antelo, S. Fiol, and F. Arce. 2014. Modeling oxyanion adsorption on ferralic soil, Part 2: Chromate, selenate, molybdate, and arsenate adsorption. Environ. Toxicol. Chem. 33:2217–2224.

Rajan S. S. S.. 1979. Adsorption of selenite, phosphate and sulphate on hydrous alumina. J. Soil Sci. 30:709–718.

Rhoades J. D. 1982. Cation exchange capacity. In: Page A. L., et al. (eds.). Methods of Soil Analysis. Part 2. Agron. Monogr. 9. 2nd ed. American Society of Agronomy, Madison, WI. pp. 149–157.

Rietra R. P. J. J., T. Hiemstra, and W. H. van Riemsdijk. 2001. Comparison of selenate and sulfate adsorption on goethite. J. Colloid Interface Sci. 240:384–390.

Rovira R., J. Giménez, M. Martínez-Lladó, J. de Pablo, V. Martí, and L. Duro. 2008. Sorption of selenium(IV) on the natural iron oxides: Goethite and hematite. J. Hazard. Mater. 150:279–284.

Secor R. B., and C. J. Radke. 1985. Spillover of the diffuse double layer on montmorillonite particles. J. Colloid Interface Sci. 103:237–244.

Sims J. T., and F. T. Bingham. 1968. Retention of boron by layer silicates, sesquioxides, and soil materials: II. Sesquioxides. Soil Sci. Soc. Am. Proc. 32:364–369.

Sposito G. 1983. On the surface complexation model of the oxide-aqueous solution interface. J. Colloid Interface Sci. 91:329–340.

Sposito G., J. C. M. de Wit, and R. H. Neal. 1988. Selenite adsorption on alluvial soils: III. Chemical modeling. Soil Sci. Soc. Am. J. 52:947–950.

Sprycha R. 1989a. Electrical double layer at alumina/electrolyte interface. I. Surface charge and zeta potential. J. Colloid Interface Sci. 127:1–11.

Sprycha R. 1989b. Electrical double layer at alumina/electrolyte interface. II. Adsorption of supporting electrolyte ions. J. Colloid Interface Sci. 127:12–25.

Su C., and D. L. Suarez. 2000. Selenate and selenite sorption on iron oxides: An infrared and electrophoretic study. Soil Sci. Soc. Am. J. 64:101–111.

Vuori E., J. Vääriskoski, H. Hartikainen, P. Vakkilainen, J. Kumpulainen, and K. Niinivaara. 1989. Sorption of selenate by Finnish agricultural soils. Agric. Ecosyst. Environ. 25:111–118.

Vuori E., J. Vääriskoski, H. Hartikainen, J. Kumpulainen, T. Aarnio, and K. Niinivaara. 1994. A long-term study of selenate adsorption in Finnish cultivated soils. Agric. Ecosyst. Environ. 48:91–98.

Weast R. C., M. J. Astle, and W. H. Beyer. 1984. CRC Handbook of Chemistry and Physics. Boca Raton, FL, CRC Press, Inc..

Wijnja H., and C. P. Schulthess. 2000. Vibrational spectroscopy study of selenate and sulfate adsorption mechanisms on Fe and Al (hydr)oxide surfaces. J. Colloid Interface Sci. 229:286–297.

Wu C.- H., S.- L. Lo, and C.- F. Lin. 2000. Competitive adsorption of molybdate, chromate, sulfate, selenate and selenite on γ-Al_2O_3. Colloids Surf. A. Physicochem. Eng. Aspects. 166:251–259.

Wu C.- H., S.- L. Lo, C.- F. Lin, and C.- Y. Kuo. 2001. Modeling competitive adsorption of molybdate, sulfate, and selenate on γ-Al_2O_3 by the triple-layer model. J. Colloid Interface Sci. 233:259–264.

Yläranta T. 1983. Sorption of selenite and selenate in the soil. Ann. Agric. Fenn. 22:29–39.

Zhang P., and D. L. Sparks. 1990. Kinetics of selenate and selenite adsorption/desorption at the goethite/water interface. Environ. Sci. Technol. 24: 1848–1856.